

Successive Correction of the Mean Sea Surface Height by the Simultaneous Assimilation of Drifting Buoy and Altimetric Data

YOICHI ISHIKAWA, TOCHIYUKI AWAJI, AND KAZUNORI AKITOMO

Department of Geophysics, Faculty of Science, Kyoto University, Kyoto, Japan

BO QIU

Department of Oceanography, University of Hawaii at Manoa, Honolulu, Hawaii

(Manuscript received 29 September 1995, in final form 9 April 1996)

ABSTRACT

A simultaneous assimilation model of drifting buoy and altimetric data is proposed to determine the mean sea surface height (SSH) as well as the temporal evolution of the surface circulation on synoptic scales. To demonstrate the efficiency of our assimilation model, several identical twin experiments for the double-gyre circulation system are performed using a $1\frac{1}{2}$ -layer primitive equation model. An optimal interpolation for the multivariate is used for the assimilation scheme that assumes the geostrophic relationship between the error fields of the velocity and the interface depth. To identify the nature of the assimilation of the buoy-derived velocities into the dynamical ocean model, the authors first conduct the assimilation experiment using the drifting buoy data alone. The result shows that realistic buoy deployment (32 in a 40° square) can effectively constrain the model variables; that is, both the absolute (mean plus time varying) velocity and SSH (interface depth) fields are significantly improved by this buoy data assimilation. Moreover, in the case of denser buoy deployment in the energetic western boundary current regions, where the mean SSH is comparable to the time-varying part and the geoid error is relatively large, the assimilation provides a better determination of the absolute velocity and SSH. This is because significant changes in the mean SSH lead to an improvement along the extensive buoy trajectories associated with the strong current. It is worth noting that the assimilation of drifting buoy data is more effective than that of moored velocity data, thanks to the Lagrangian information content of the drifting buoys. Successive correction of the mean SSH is made with simultaneous assimilation of drifting buoy and altimetric data. Consequently, a better correction of the mean SSH is obtained: The initial error of the mean SSH is reduced by approximately 40% after the 1-year experiment. In contrast, the assimilation experiment of altimetric data alone corrects only the time-varying part, but yields little error reduction for the mean SSH in our model. These results clearly show that the simultaneous assimilation of drifting buoy and altimetric data into the dynamical model is a very useful tool for improving the model's realism.

1. Introduction

The sea surface height (SSH) data from satellite altimeters are very attractive for physical oceanographers because of their global coverage and temporal repetition. Their potential use in monitoring mesoscale to large-scale ocean circulation and in improving its predictability through numerical modeling is a subject of increasing interest. Although several previous studies have shown this ability successfully using 4D data assimilation models (Holland and Malanotte-Rizzoli 1989; White et al. 1990; Mellor and Ezer 1991), problems remain that require improvements in assimilating the altimeter data into our models. One major problem

is that the geoid, which has geographical height variations much greater than those of the oceans, is not known on a length scale of a few hundred kilometers. Lack of accurate geoid information has limited most studies based on altimetric data to focus on either the time-varying components of the SSH or the basin-scale circulation patterns (e.g., Stammer and Wunsch 1994; Rapp et al. 1994; Le Traon et al. 1994; Nerem et al. 1994). For many oceanographic applications, an accurate mean SSH with a length scale of several hundred kilometers is required. This is particularly true for the western boundary current and its extension regions where spatial changes of the mean SSH are comparable to those of the time-varying ones.

Several methods have been proposed to deduce the mean SSH field. Mellor and Ezer (1991) and Ezer et al. (1993) showed several ways of reconstructing the mean SSH from model averages. Their approach is good as a first guess for the mean SSH field because it is defined for every grid point, but the accuracy of the

Corresponding author address: Dr. Yoichi Ishikawa, Department of Geophysics, Faculty of Science, Kyoto University, Kyoto 606, Japan.
E-mail: ishikawa@kugi.kyoto-u.ac.jp

estimated mean SSH field is doubtful for precise use. Kelly and Gille (1990) presented an approach for estimating the mean SSH in the eastward-flowing Gulf Stream on the basis of a kinematic jet model, which was extended by Qiu et al. (1991) to include recirculation gyres. There are, however, some restrictions in the application of these methods to the real ocean: For example, use of the kinematic jet model is limited to jetlike current regions such as the Gulf Stream and the Kuroshio Current.

A different attempt was made to estimate the mean SSH field based on historical hydrographic data (Willebrand et al. 1990; Capotondi et al. 1995). Since the mean SSH derived from the climatological hydrographic data covers the global ocean, this method is more applicable than those mentioned above. However, the estimated mean SSH field involves errors due to the uncertainty of specifying the reference velocities, and this may lead to significant errors in the velocity field (or the spatial change of the SSH). Differences in the averaging period are another major error source because the mean SSH field for a particular altimetric mission is averaged over a period of a few years, whereas climatological data is averaged over a period of decades. Interannual variability in the ocean circulation imposes a serious aliasing problem in estimating the mean SSH field (Qiu 1994). Several studies have tried to improve the mean SSH field estimated from the climatological dataset. For example, Willebrand et al. (1990) used information from drifter data to reduce the uncertainty in the altimetric SSH. The drifting buoy is one of the most effective means for observing the surface current because it measures the in situ absolute velocity. In their study, the altimetric data, when combined with the drifting buoy data, provide a better SSH field estimation although limited to areas where drifter data are available. It should be noted that in relating the SSH field to the buoy trajectories, geostrophic balance is usually assumed, although contributions from the ageostrophic components in regions of the western boundary currents can be substantial.

Marshall (1985) proposed an assimilation model of altimetric data to improve the geoid model as well as to obtain the ocean circulation field. His model has an advantage that the geoid model is corrected successively as new observations become available. Although a substantial decrease of error in both geoid and SSH field is achieved in a test of the model, some geoid errors still remain, especially with scales similar to those dominant in the SSH field [namely, $\sim O(100)$ km]. This is troublesome because our concern about the geoid is on scales of the ocean circulation.

In this study, the model of Willebrand et al. (1990) and Marshall (1985) will be combined and extended. The mean SSH field from the climatological hydrographic data or the model average is corrected by assimilating velocities derived from the drifting buoy data in addition to the altimetric data to overcome de-

ficiencies in these previous studies. When the velocity and SSH data are assimilated, the ageostrophic component of the velocity is considered. By using this assimilation model, an absolute SSH can be obtained not only in regions where the drifting buoy data are available, but in the nearby regions. The error of mean SSH field is expected to be corrected by the velocity data over all wavelengths of our concern.

To estimate the absolute SSH from drifting buoy and altimetric data, we adopt the identical twin approach, which uses the model-simulated results as the "observations" instead of real measurements (hereafter the "model-simulated data" are called "observation data"). Although the identical twin experiment has a tendency to give an optimistic result because of neglecting the model's deficiencies and data errors, it has the advantage that the true state of the idealized ocean is fully known. To carry out several case studies, the model is set as simply as possible; a 1½-layer, primitive equation model is used, in which the time-varying interface depths are regarded as the altimetric data (SSH). The assimilation scheme of optimal interpolation for multivariate (Daley 1991) is adopted, which is formulated with an assumption that the error field of the velocity data and that of the SSH data are geostrophically related. It should be noted that geostrophic relationship is assumed for only the error field, and hence the velocity field derived from the assimilation includes the ageostrophic components. The method of successive correction of the mean SSH field follows Marshall (1985), which is similar to the optimal interpolation.

This paper is organized as follows. In section 2, the configuration of the assimilation model is summarized including a description of the numerical model and the assimilation scheme. Section 2 also gives the description of the control run and simulation run associated with the configuration of the identical twin experiment. In section 3, results of the identical twin experiments are shown, including the drifting buoy assimilation, the simultaneous assimilation of drifting buoy and altimetric data, and the successive correction of the mean SSH field. In section 4, we discuss the effectiveness of the successive correction model as well as the assimilation of the drifting buoy data and summarize the result of our experiment. The outlook for the future development of this model is also discussed.

2. Assimilation model

a. Numerical model

The model basin is a rectangular ocean of 40° width in both latitude and longitude that idealizes the western part of the North Pacific. The governing equations are familiar ones of a 1½-layer reduced gravity model as follows:

$$\frac{\partial u}{\partial t} + L(u) - \frac{uv \tan \phi}{R} - fv = -\frac{g'}{R \cos \phi} \frac{\partial h}{\partial \lambda} + \frac{\tau_\lambda}{\rho_0(H+h)} + F_\lambda \quad (1)$$

$$\frac{\partial v}{\partial t} + L(v) - \frac{u^2 \tan \phi}{R} + fu = -\frac{g'}{R} \frac{\partial h}{\partial \phi} + \frac{\tau_\phi}{\rho_0(H+h)} + F_\phi \quad (2)$$

$$\frac{\partial h}{\partial t} + \frac{1}{R \cos \phi} \left\{ \frac{\partial(H+h)u}{\partial \lambda} + \frac{\partial(H+h)v \cos \phi}{\partial \phi} \right\} = 0, \quad (3)$$

where L is the advective operator and F_λ, F_ϕ are the friction terms for the zonal and meridional velocity components, respectively:

$$L(\mu) = \frac{1}{R \cos \phi \cdot (H+h)} \left\{ \frac{\partial(H+h)\mu}{\partial \lambda} + \frac{\partial(H+h)v\mu \cos \phi}{\partial \phi} \right\} \quad (4)$$

$$F_\lambda = \frac{A_H}{R^2 \cos^2 \phi} \left\{ \frac{\partial^2 u}{\partial \lambda^2} + \cos \phi \frac{\partial}{\partial \phi} \left(\cos \phi \frac{\partial u}{\partial \phi} \right) + (\cos^2 \phi - \sin^2 \phi) u - 2 \sin \phi \frac{\partial v}{\partial \lambda} \right\} \quad (5)$$

$$F_\phi = \frac{A_H}{R^2 \cos^2 \phi} \left\{ \frac{\partial^2 v}{\partial \lambda^2} + \cos \phi \frac{\partial}{\partial \phi} \left(\cos \phi \frac{\partial v}{\partial \phi} \right) + (\cos^2 \phi - \sin^2 \phi) v + 2 \sin \phi \frac{\partial u}{\partial \lambda} \right\}. \quad (6)$$

The boundary conditions are as follows. A no-slip condition is imposed along the model's lateral boundaries. At the sea surface, steady wind stresses, τ_λ and τ_ϕ , are applied,

$$(\tau_\lambda, \tau_\phi) = \left(-\tau_0 \cos \left(2\pi \frac{(\phi - \phi_0)}{L_\phi} \right), 0 \right) \quad (7)$$

so as to force a double-gyre circulation. In order to conduct a twin experiment, random wind stresses with magnitude of 20% of its amplitude are added to τ_λ in the control run. In the simulation and assimilation runs, no random stresses are added to Eq. (7). Since our aim of the experiment is to examine the efficiency of the new approach to estimate the mean SSH field, the different wind stresses are used in the control run and the assimilation run to make the different mean SSH field. The values of parameters used here are summarized in Table 1.

TABLE 1. Parameters in the numerical model.

(L_λ, L_ϕ)	Model region	(40°, 40°)
ϕ_0	Latitude of southern boundary	15°
(d_λ, d_ϕ)	Grid size	(1/12°, 1/12°)
f	Coriolis parameter (at 35°N)	$2\Omega \sin \phi$ ($8.4 \times 10^{-5} \text{ s}^{-1}$)
g'	Reduced gravity	1.96 cm s^{-2}
R	Radius of the earth	6370 km
H	Upper-layer thickness	600 m
A_H	Horizontal viscosity	$5.0 \times 10^6 \text{ cm}^2 \text{ s}^{-1}$
τ_0	Amplitude of the wind stress	1.0 dyn cm^{-2}
a	Rossby radius of deformation	40.8 km at 35°N

A 12-year spinup integration is performed using a grid spacing of $\frac{1}{4}^\circ$, followed by a 10-year integration with a finer ($\frac{1}{12}^\circ \times \frac{1}{12}^\circ$) grid. After the 22-year integration, the model state is nearly in dynamic equilibrium. Figure 1 shows the schematic diagram of the model spinup and the identical twin experiment. For the control run, an additional 6-year integration is performed with the wind stresses including random components, and its final output is used as the initial state (Fig. 2a). The 1-year experiment of the control run, calculated from this initial state, is regarded as the true ocean that gives the "observations." The mean interface depth (1-year average) of the control run is shown in Fig. 2b, which is subtracted from the absolute interface depth to make the time-varying part used as the altimetric observation (see next section). The result of the control run is also used to assess the success of the assimilation result quantitatively. We define the rms error as

$$\text{rms}_{\text{experiment}} = \left(\frac{1}{N} \sum_{n=1}^N (w_{\text{experiment}} - w_{\text{control}})^2 \right)^{1/2}, \quad (8)$$

where w represents each variable and N is the number of the variables of rms calculated; for example, all grid numbers for the global rms error.

For the assimilation run and the simulation run, a 1-year integration is added to the 22-year spinup to make the initial state (Fig. 3a). Thus, the initial condition of these assimilation and simulation runs is different from that of the control run. The 1-year experiment of the simulation run is calculated under the same conditions as the assimilation run (initial condition and wind stress) except that the observation data are not assimilated. The simulation run is used as the reference to evaluate the success of the assimilation. It also gives the first guess of the mean interface depth field (Fig. 3b), idealizing the estimated mean SSH field from the climatological data. In Fig. 3c, the difference of the mean interface depth between the control run and the simulation run (the mean interface depth error of the simulation run) is shown. Large errors can be seen in the western boundary current and its extension regions. The mean eastward jet in the simulation run is weaker

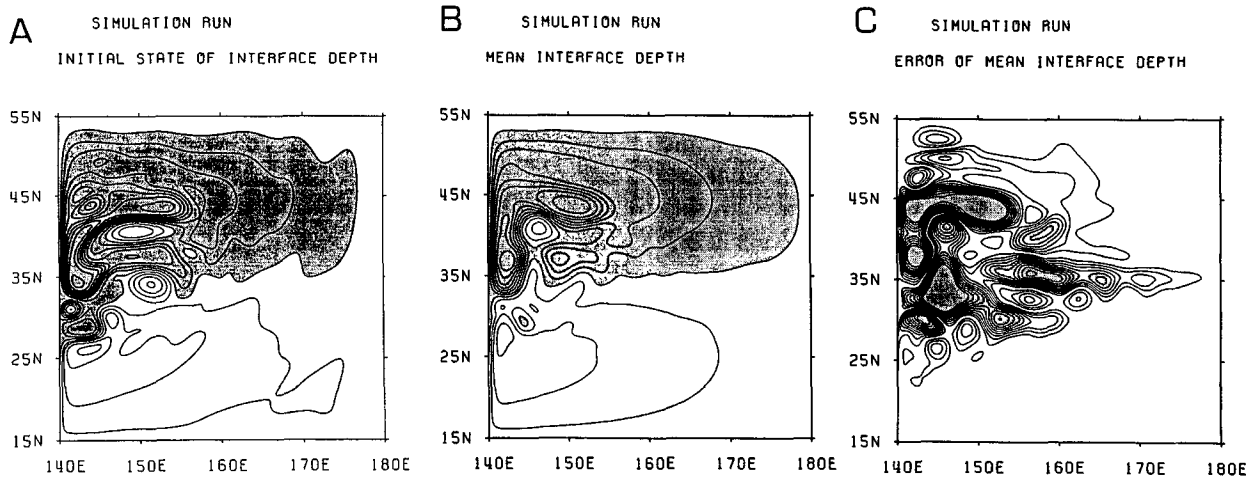


FIG. 3. (a) The initial state of the interface depth field for assimilation and simulation runs and (b) mean interface depth of the simulation run. Contour interval is as in Fig. 2. (c) Mean interface depth error of the simulation run. Contour interval is 20 m. The light (dark) shaded parts represent the region where the error is greater than 100 m (180 m).

than that of the control run (Figs. 2b and 3b), and this is due to the large error in the extension region.

b. Model-simulated data

The data assimilated into the model are derived from the result of the control run in this study. The velocity data are based on particle trajectories (regarded as observed buoy trajectories) tracked in the control run using the Euler–Lagrangian technique (Awaji et al. 1991). Using these particle trajectories, the velocities at particle positions are estimated daily by

$$u_i(x_i(n), y_i(n)) = \frac{x_i(n+1) - x_i(n-1)}{2\Delta t}$$

$$v_i(x_i(n), y_i(n)) = \frac{y_i(n+1) - y_i(n-1)}{2\Delta t}, \quad (9)$$

where Δt is a time interval (1 day) and $x_i(n)$ and $y_i(n)$ are the positions on day n for the i th particle. These velocities derived from the buoy data differ from the velocities of the control run because they are the two-day Lagrangian average. The differences, however, are less than 1 cm s^{-1} in the western boundary current regions and can be ignored in this study.

We also derive the velocity data from moored current meters. These are taken directly from the daily velocity field of the control run. The altimetric data are sampled every 17 days from the interface depth anomaly field along the assumed Geosat subtracks (shown in Fig. 4) in the control run. Here the anomaly field is the deviation from the 1-year mean interface depth shown in Fig. 2b.

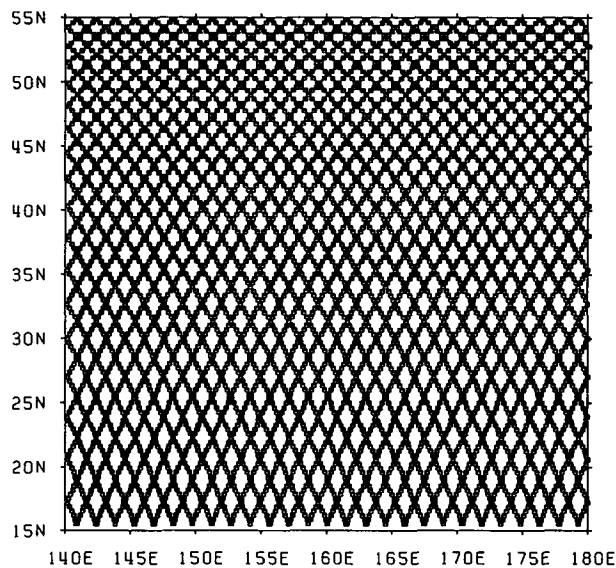


FIG. 4. The assumed Geosat subtracks.

TABLE 2. Parameters used in the assimilation.

Nudging method		
T_a	Timescale (strength of the nudging term)	0.1 day
T_d	Dumping timescale of the nudging term	1 day
R_{nudge}	Dumping lengthscale	40 km
Optimal interpolation		
ϵ	Ratio of the model error to the observation error	1
R_{OI}	Correlation scale of the model error	160 km
N	Number of the assimilated data	30

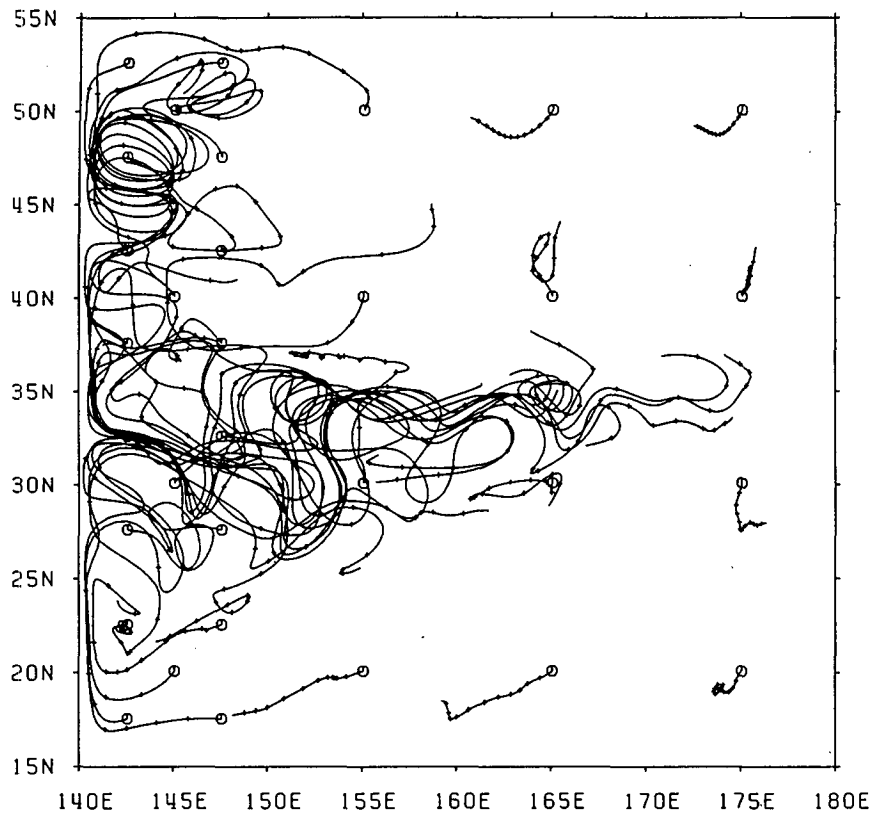


FIG. 5. Spaghetti diagram of buoy trajectories for expt 1-4. Small circles indicate the initial points, where velocity data are observed as moored data in expt 1-5.

c. Assimilation scheme

1) NUDGING METHOD

To assimilate the velocity data derived from drifting buoys or moored current meters into the model in experiment 1 described later, we introduce the nudging term in the equation of motion as

$$\frac{\partial u}{\partial t} = (\text{physics}) - \lambda(u - u^o), \quad (10)$$

where (physics) represents all terms in the 11/2-layer primitive equations [Eqs. (1) and (2)] except for the time-derivative terms. Following Holland and Malanotte-Rizzoli (1989) and Haines et al. (1993), the nudging factor λ is given by

$$\lambda = \begin{cases} \frac{1}{T_a} \exp\left(-\frac{r^2}{R_{\text{nudge}}^2}\right) \exp\left(-\frac{t-t^o}{T_d}\right), & r \leq 4R_{\text{nudge}} \\ 0, & r > 4R_{\text{nudge}}, \end{cases} \quad (11)$$

where r is the distance between the grid point in the model and the observation point (buoy position) and $(t - t_0)$ is the difference between the observation and

assimilation time. Here T_a is the timescale, which determines the strength of the nudging factor, and T_d is the dumping timescale for the nudging term.

The reason that the nudging method is adopted is simply to save computational time. In addition, the number of the buoy data assimilated in this study is not so many: When considering Eq. (11), we can obtain the information from at most one buoy near each grid point.

2) OPTIMAL INTERPOLATION FOR MULTIVARIATE

The optimal interpolation (OI) method used in many previous studies for the assimilation of altimetric data (Marshall 1985; Mellor and Ezer 1991; Ezer and Mellor 1994) is extended here to assimilate the drifting buoy and altimetric data simultaneously (Daley 1991; Ghil and Malanotte-Rizzoli 1991).

The analysis value \mathbf{w}^a is obtained from the model calculated value \mathbf{w}^f and the observed value \mathbf{w}^o through Eq. (12):

$$\mathbf{w}^a = \mathbf{w}^f + K(\mathbf{w}^o - H\mathbf{w}^f), \quad (12)$$

where \mathbf{w} is the column vector for all variables, $\mathbf{w} = (h \ u \ v)^T$, and H is the observation matrix that trans-

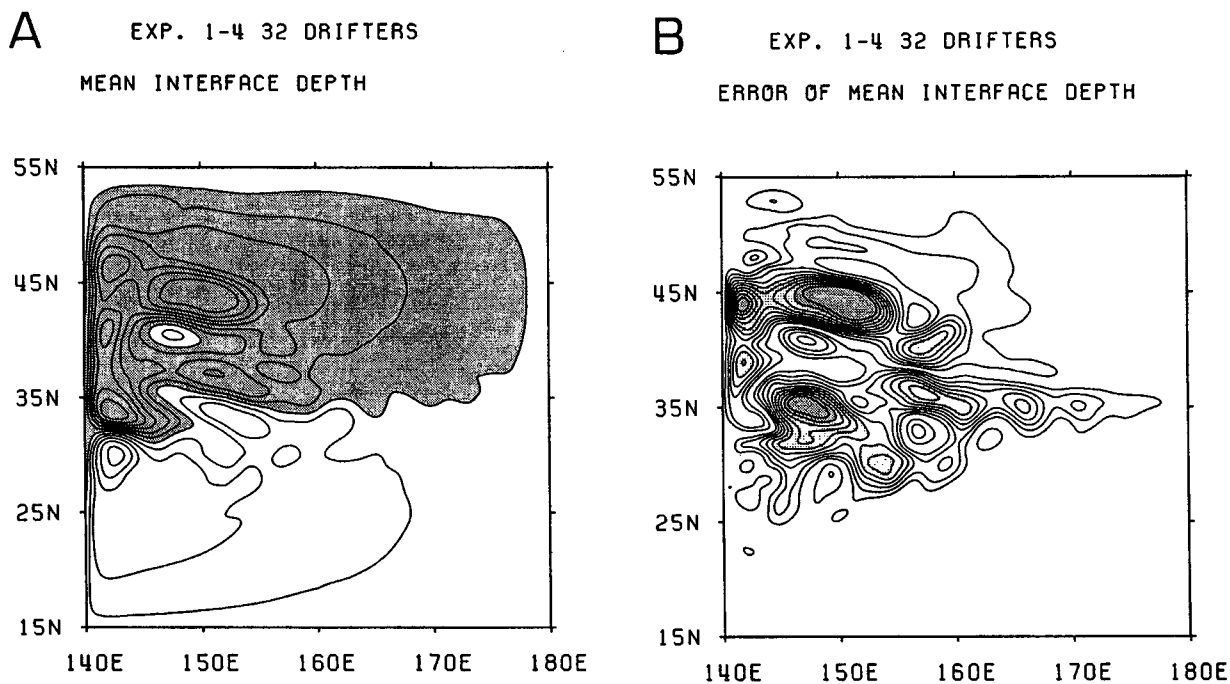
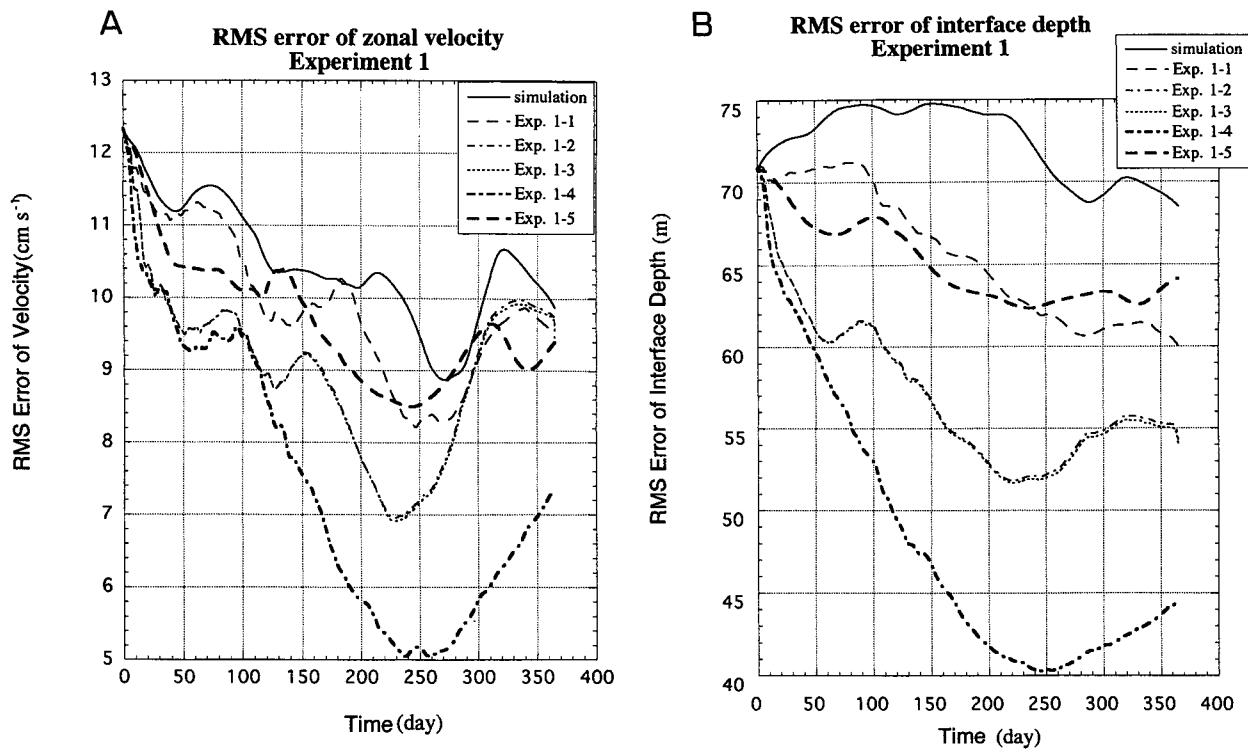


TABLE 3. Summary of the experiments.

Experiments	Number of buoys	Altimetric data	Assimilation scheme	Successive correction of mean SSH	Error of estimated mean SSH (m)
Control Simulation	—	—	—	—	—
1-1	16	no	nudging	no	60.1
1-2	24	no	nudging	no	55.6
1-3	32	no	nudging	no	55.6
1-4	32	no	nudging	no	48.5
1-5	32 (moored)	no	nudging	no	59.9
2-1	no	yes	OI	no	63.5
2-2	32	yes	OI	no	58.8
3-1	no	yes	OI	yes	64.3
3-2	32	yes	OI	yes	38.7

forms the forecast data to the values at the observed points. The observation of the interface depth, h^o , is used for the estimated mean field plus the time-varying part derived from the altimeter (in this sense, the total SSH derived from the altimeter is assimilated into the model).

The matrix K is determined to minimize the error of the analysis field (Ghil and Malanotte-Rizzoli 1991):

$$K = P^f H^T (HP^f H^T + R^o)^{-1} \quad (13)$$

where the P^f, R^o are the error covariance matrices for the forecast and observed values, respectively, and are assumed as

$$P^f = \begin{pmatrix} C_{hh} & C_{hu} & C_{hv} \\ C_{uh} & C_{uu} & C_{uv} \\ C_{vh} & C_{vu} & C_{vv} \end{pmatrix}, \quad R^o = \epsilon I, \quad (14)$$

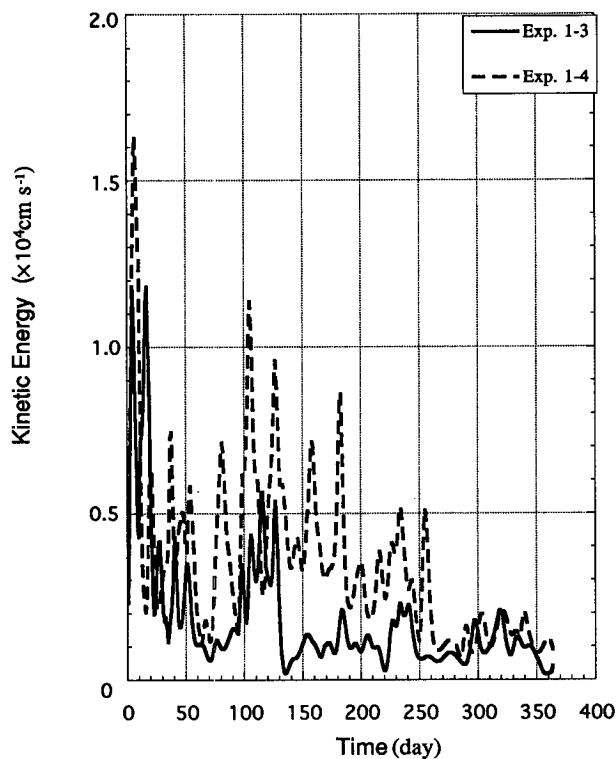


FIG. 8. The kinetic energy $[(u^2 + v^2)/2]$ derived from the buoy-observed data in expts 1-3 and 1-4.

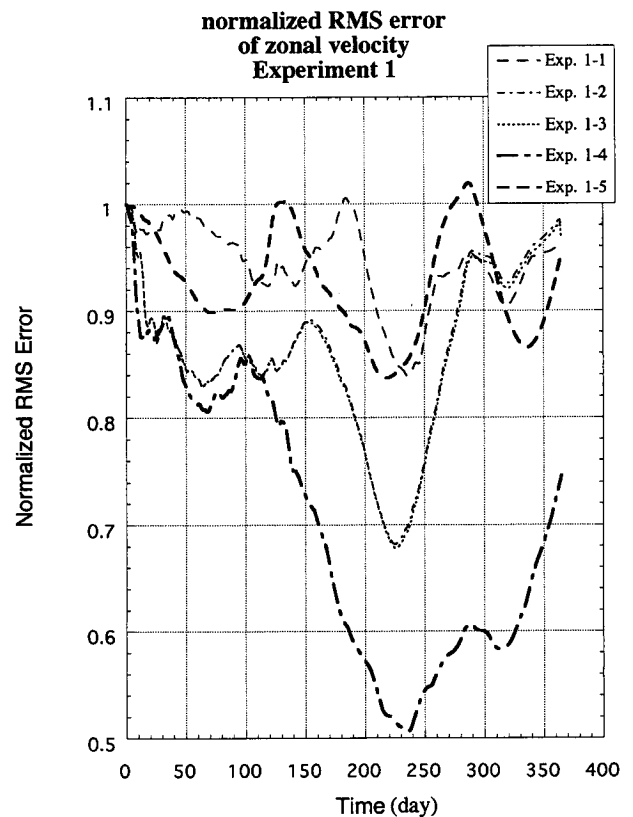


FIG. 9. The time series of normalized rms errors for zonal velocity in expt 1.

where ϵ is the error variance ratio of the model forecast and the observation, assumed to be 1 in this study, and I is the unit matrix.

The model error covariance matrix is assumed to be a Gauss function for the interface depth and is obtained from the geostrophic relationship between the interface depth field and the velocity field:

$$C_{hh} = \exp\left\{-\frac{(x_1 - x_2)^2 + (y_1 - y_2)^2}{R_{OI}^2}\right\} \quad (15)$$

$$C_{hu} = -C_{uh} = -2 \frac{g'}{f} \frac{(y_1 - y_2)}{R_{OI}^2} C_{hh} \quad (16)$$

$$C_{hv} = -C_{vh} = 2 \frac{g'}{f} \frac{(x_1 - x_2)}{R_{OI}^2} C_{hh} \quad (17)$$

$$C_{uu} = \left(\frac{g'}{f}\right)^2 \frac{2}{R_{OI}^2} \left\{1 - \frac{2(y_1 - y_2)^2}{R_{OI}^2}\right\} C_{hh} \quad (18)$$

$$C_{vv} = \left(\frac{g'}{f}\right)^2 \frac{2}{R_{OI}^2} \left\{1 - \frac{2(x_1 - x_2)^2}{R_{OI}^2}\right\} C_{hh} \quad (19)$$

$$C_{uv} = C_{vu} = \left(\frac{g'}{f}\right)^2 \left(\frac{2}{R_{OI}^2}\right)^2 (x_1 - x_2)(y_1 - y_2) C_{hh}. \quad (20)$$

The values of all parameters used for the assimilation are listed in Table 2.

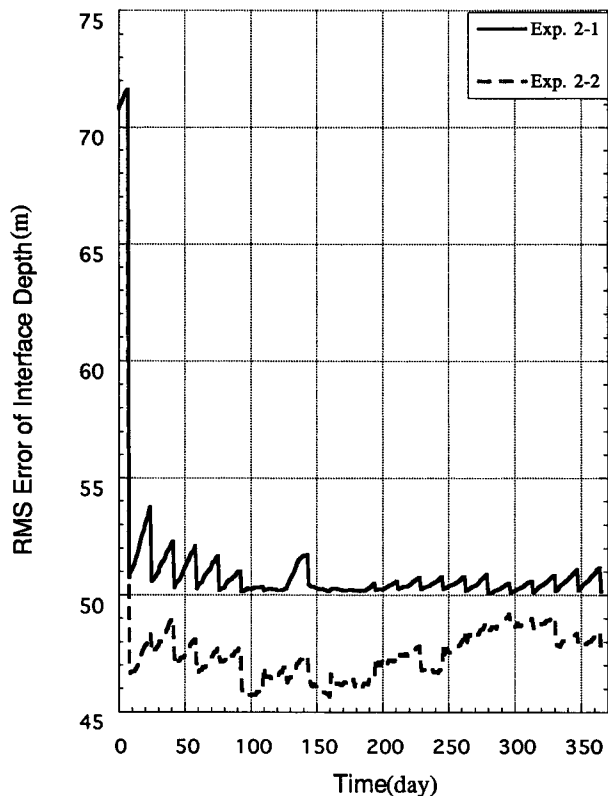


FIG. 10. Time series of the rms errors for interface depth in expt 2.

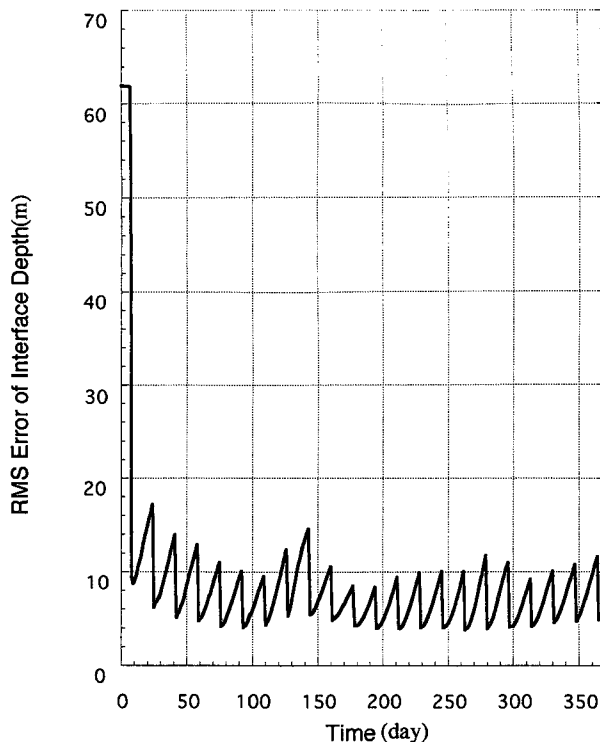


FIG. 11. Time series of the rms error of the time-varying part of interface depth in expt 2-1.

3. Assimilation of the buoy and altimetric data

a. Experiment 1: Assimilation of the buoy data

The efficiency of assimilating drifting buoy data should be confirmed before the simultaneous assimilation of the buoy and altimetric data is carried out since it is considered to determine the success of the estimation and the correction of the mean SSH field. The efficiency to assimilate the velocity data is indicated by Fukumori and Malanotte-Rizzoli (1995) and Malanotte-Rizzoli and Young (1992) who assimilated moored velocity data into idealized Gulf Stream models. The main advantage of assimilating velocity data is the inclusion of the ageostrophic information, which becomes very important in the Gulf Stream region.

We examine, at first, the effectiveness of only drifting buoy data assimilation with the different number or the initial positions through the following five cases. After dividing the model ocean into $10^\circ \times 10^\circ$ square regions (16 squares), one particle is deployed at the center of each region in experiment 1-1. In experiment 1-2, 24 particles are used, of which 16 particles are deployed in the same manner as in experiment 1-1 and 8 particles are randomly added near the western boundary. In experiment 1-3, 8 particles are deployed in the eastern domain in addition to the particle deployment in experiment 1-2. In experiment 1-4, 32 particles, the

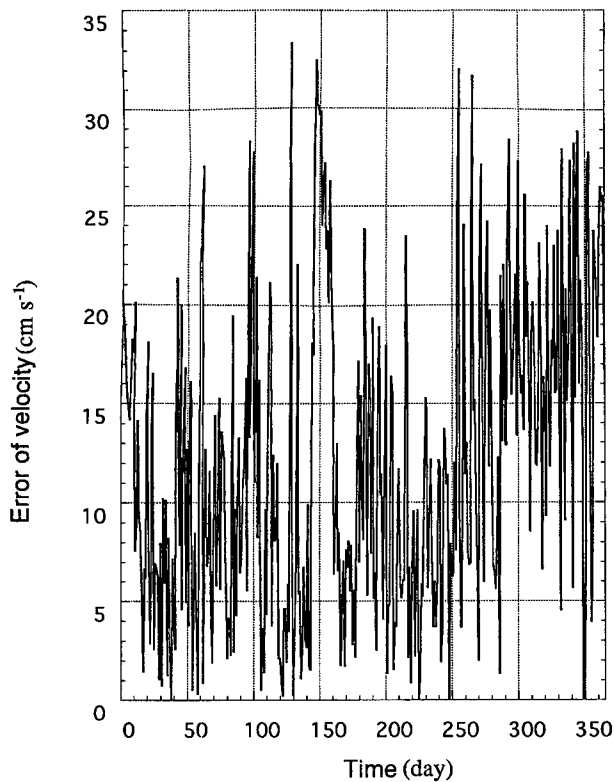


FIG. 12. Time series of the zonal velocity error at a fixed point (35°N, 142.5°E) in expt 2-2.

same number as in experiment 1-3, are deployed but at different initial positions. Sixteen of the 32 particles are deployed in the same position as in experiment 1-1. The remaining 16 particles are placed at the center of 16 subregions ($5^\circ \times 5^\circ$ blocks) into which the western quarter of the model region (from 140° to 150° E) is divided. In experiment 1-5, the initial points of the data are set the same as in experiment 1-4 but the data points are fixed geographically to simulate the effect of the moored data. The spaghetti diagram of the buoy trajectories for experiment 1-4 over a period of 1 year is shown in Fig. 5.

The time series of the rms errors for the zonal velocity (u) and the interface depth (h) fields are shown in Fig. 6. In each case, the errors in both the velocity and the interface depth field can be substantially corrected, despite the fact that the nudging term is added to the momentum equation only. This shows that the realistic number of the buoys in this region can constrain not only the velocity field but also the interface depth field through the model dynamics. This result suggests that the assimilation of the drifting buoy data is effective in estimating the mean interface depth. In practice, the 1-year-averaged mean interface depth field is closer to the mean field of the control run than that of the simulation run. The maps of the mean interface

depth field and its error for experiment 1-4 are shown in Fig. 7 and the rms errors for each case are summarized in Table 3.

A careful comparison among these cases reveals several interesting points. First, it is related to the initial deployment of the drifting buoys. The error of the experiment could be expected to reduce when the number of the buoy data increases, but there is little difference between experiments 1-2 and 1-3. Moreover, the reduction rate of the rms error in experiment 1-4 is twice as much as in experiment 1-3, which had the same number of buoys but started from different initial positions. The following reason can be conjured for this strong dependency of the buoy deployment. The energy input by the nudging term is larger in experiment 1-4 than in experiment 1-3. The time series of the sum of the kinetic energy $(u^2 + v^2)/2$ of the observation data is shown in Fig. 8; though not equal, this provides a measure for the intensity of the nudging term. Together with this, the spatial distribution of the error field (Fig. 3c) shows large values in the western boundary current and its extension regions. The observation data in the large error region can correct more effectively than in the small error region because of the large energy input by the nudging term $(u - u^o)$ [see Eq. (10)].

Second, the effectiveness of the drifting buoy data assimilation (expt 1-4) is confirmed by comparing with

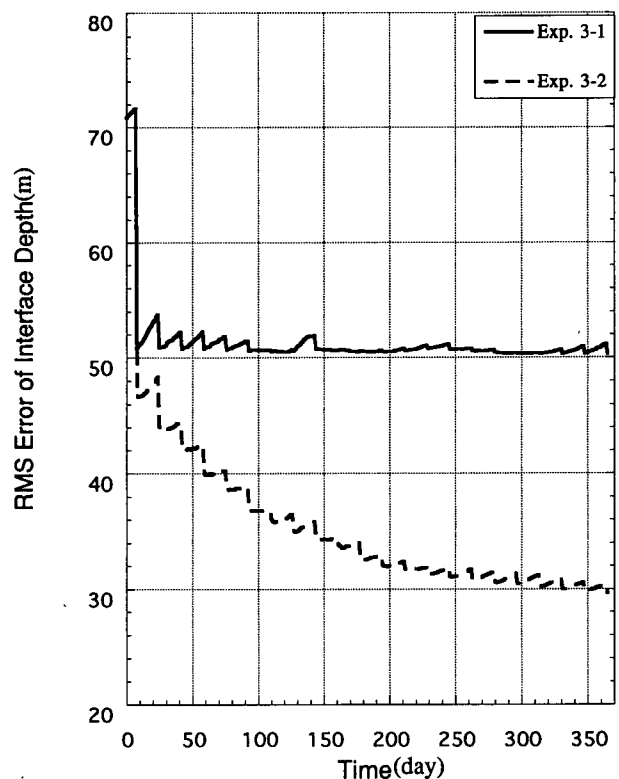


FIG. 13. As in Fig. 10 but for expt 3.

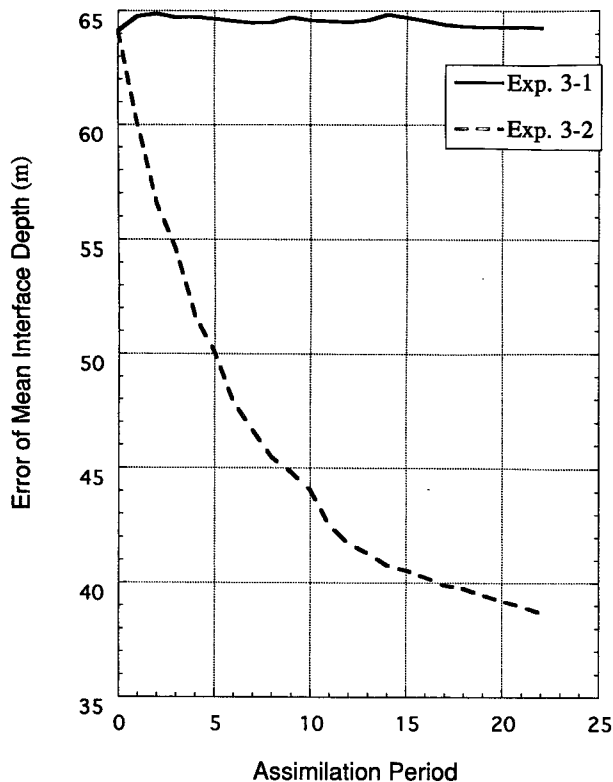


FIG. 14. Errors of the estimated mean interface depth at each assimilation period in expt 3.

the moored data assimilation (expt 1-5). In experiment 1-5, much larger errors appear, suggesting the velocity data from moored current meters are less effective for the assimilation than the buoy-derived velocity data. The effectiveness of the drifting buoy data can be explained by considering the contribution that carries the observed information. Malanotte-Rizzoli and Young (1992) noted that the information of localized data can constrain the model through circulation advection and wave propagations. Assimilation of the velocities derived from the drifting buoys is expected to have an additional effect as they provide the Lagrangian information.

In Fig. 6, the time evolution of all assimilation experiments shows a similar trend to that of the simulation run (no assimilation). This is due to the intrinsic variability of the unconstrained model because the deployment of the drifting buoys is rather sparse even in experiment 1-4, the case of the largest number of the drifting buoys. In fact, the grid number with the buoy data assimilated in experiment 1-4 is only 15% of the total grid number. Such a background trend in the assimilation experiments is most conspicuous in experiment 1-1, which has the smallest buoy number, but decreases with increasing of the buoy number. This suggests that when the buoy observations are dense es-

pecially in the region of dynamical activity, the buoy data assimilation becomes effective in decreasing the rms error in the assimilation run. To assess this unambiguously, we normalized the rms errors of all assimilation experiments by the rms error of the simulation run. Similar approaches have been used by Malanotte-Rizzoli and Young (1992) and Fukumori and Malanotte-Rizzoli (1995). As shown in Fig. 9, the normalized rms error for the velocity field in experiment 1-4 decreases down to 0.5 on day 240. This confirms that the decrease of the rms error in the assimilation run (Fig. 6) is mainly attributed to the success of the assimilation.

In all assimilation experiments except for experiment 1-5, however, there is a significant increase in both the rms errors (Fig. 6) and its normalized ones (Fig. 9). This is related to the small kinetic energy of velocities experienced by the drifting buoys during the last 100 days of the assimilation (Fig. 8) when most of the buoys moved away from the western boundary region. More discussions concerning this point will be given in section 4.

b. Experiment 2: Simultaneous assimilation of the buoy and the altimetric data

It is useful to examine the characteristics of the altimetric data assimilation and efficiency of the simultaneous assimilation of both drifting buoy and altimetric data before the successive correction model of the mean SSH is carried out.

In the first case (expt 2-1), only the altimetric data are assimilated as the reference, and the characteristic of the altimetric data assimilation is examined. The simultaneous assimilation of the buoy and altimetric data is carried out as the second case (expt 2-2). In both cases, the 1-year average of the simulation run is used for the estimated mean interface depth (Fig. 3b), which has the rms error of 64.1 m (corresponding to about 13 cm in SSH). The buoy data used in experiment 2-2 are the same data as used in experiment 1-4, and all data observed after the previous assimilation period are assimilated at the same time with the altimetric data, every 17 days, without considering the time lag.

The time series of the rms errors for the interface depth are shown in Fig. 10. The most visible result of both cases is that the error level of the interface depth field does not change so much during the assimilation period. This is because the error of the mean interface depth field contaminates the analysis field at each assimilation time. Thus, the time-varying part of the observed interface depth corrects only the time-varying part of the model output and cannot constrain the mean field of the model on synoptic scales. In practice, the rms error for the time-varying part in experiment 2-1 (Fig. 11) is reduced to about 10 m, while the error for the absolute interface depth (mean plus time-varying part) is reduced to 50 m, indicating that the error of the

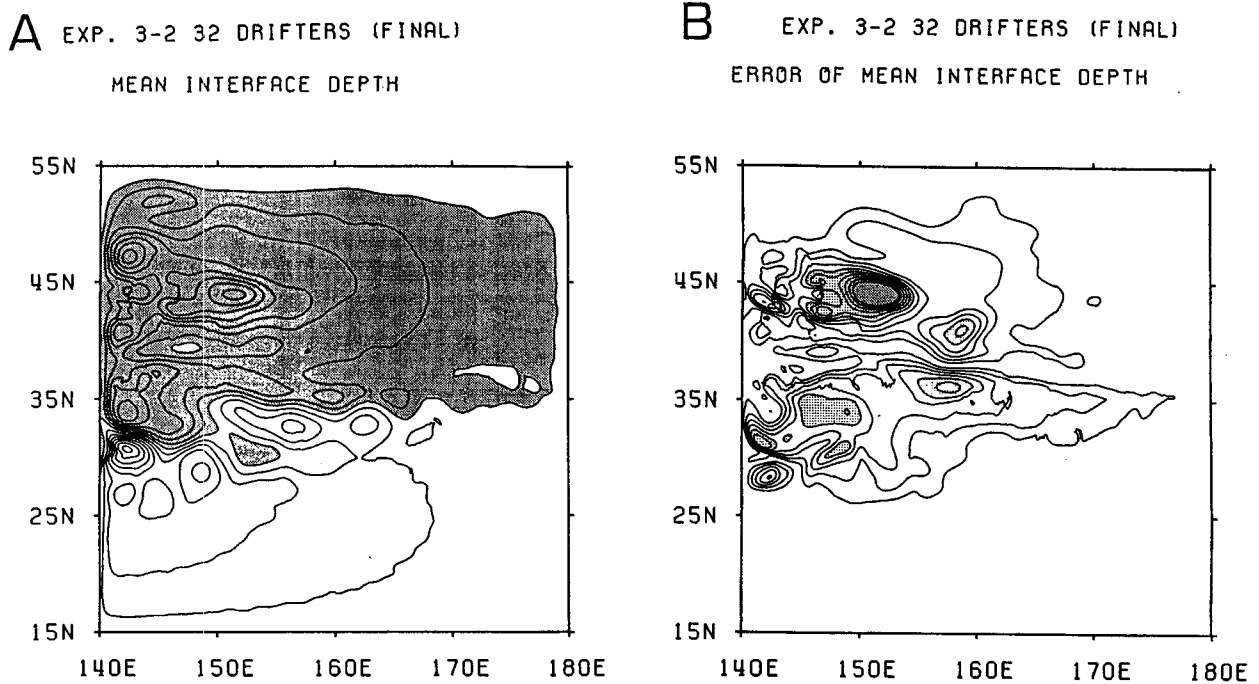


FIG. 15. (a) The estimated mean interface depth and (b) its error at the final assimilation time in expt 3-2. Contour intervals as in Fig. 3.

mean interface depth is the major part in the absolute interface depth error. This result is consistent with that of Capotondi et al. (1995) who used the Geosat data combining the hydrographic mean field. They showed that the assimilation of altimetric data alone cannot constrain the mean field of the model. The error of the mean SSH field summarized in Table 3 does not change from the initial guess in experiment 2-1, when only the altimetric data are assimilated.

The simultaneous assimilation of buoy and altimetric data (expt 2-2) can reduce the error of the interface depth field in contrast to experiment 2-1. This shows that the drifting buoy data are effective in correcting the SSH field, which is also indicated in the previous subsection. The error of the velocity is not reduced sufficiently, especially in the latter half of the experiment period (not shown). The velocity field is related not to the interface depth field but to its gradient, and the small-scale undulation in the analyzed SSH field can generate gravity waves that diminish the effect of the buoy assimilation. Several sources for the gravity waves exist. The most crucial one is the error of the mean SSH field, which causes dynamical inconsistency in the observation data. The time evolution of the velocity error at 35°N, 142.5°E is shown in Fig. 12 and the persistent existence of the gravity waves is clearly indicated. These waves are related to the error of the observed altimetric data (mean plus time-varying part). The time evolution of the interface depth error at the same point (not shown) has the peak at the as-

simulation time due to the contamination of the error in the mean interface depth field. This situation is expected to be improved when the mean SSH field is corrected.

From these experiments, we found that it is important to use accurate mean SSH to assimilate the altimetric data and the simultaneous assimilation of the drifting buoy and altimetric data is effective in constraining the SSH field. It is expected that the mean SSH field can be corrected successively with the simultaneous assimilation of the drifting buoy and altimetric data. The result for the successive correction of the mean SSH field is described in section 3c with its method.

c. Experiment 3: The model for the successive correction of mean SSH

The formulation used here follows Marshall (1985). Since Marshall (1985) focused on improving the geoid field whereas this study attempts to correct the mean interface depth, a slight modification is needed.

The formulation of the basic equation is similar to the optimal interpolation in section 2c(2):

$$\bar{h}^+ = \bar{h}^- + K'(h^f - h'^o - \bar{h}^-). \quad (21)$$

The notation is the same as in Eq. (12), where \bar{h} is the mean interface depth, superscripts $^+$ and $^-$ are the corrected and a priori estimation of the mean interface

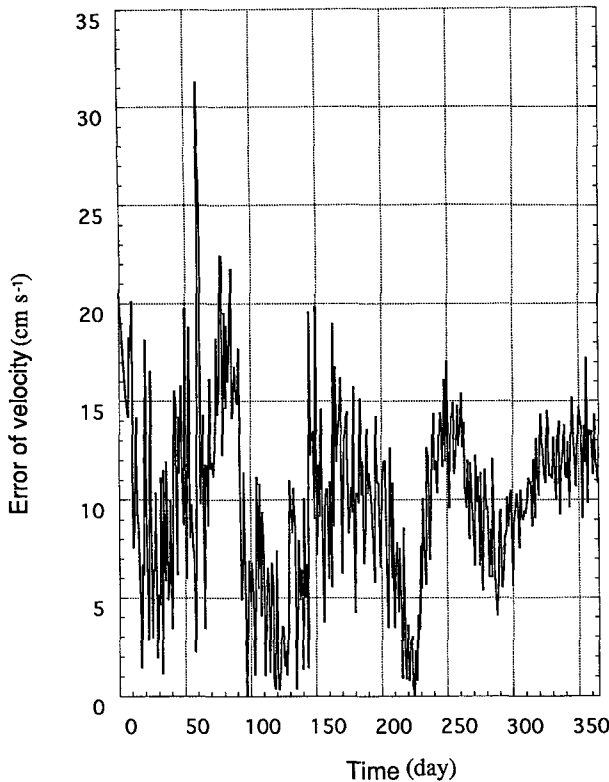


FIG. 16. As in Fig. 12 but for expt 3-2.

depth, and h'^o is the observed time-varying part of the interface depth.

With the assumption that the time-varying part has no error and that the error of the mean SSH is uncorrelated spatially, K' becomes

$$K' = (R'^o + \bar{R}^o)(HP^fH^T + R'^o + \bar{R}^o)^{-1} = I - K. \tag{22}$$

The second transform is from comparing with Eq. (13) and using Eq. (12) because of $R'^o = 0$ and R^o in Eq. (13) is equal to \bar{R}^o , where R'^o and \bar{R}^o are error covariance matrices of the altimetric observation and the estimated mean SSH field, respectively. From Eq. (22) the new estimation for the mean SSH field is obtained:

$$\bar{h}^+ = \bar{h}^- + (I - K)(h^f - h'^o - \bar{h}^-) = h^a - h'^o, \tag{23}$$

where h^a is the analysis value of the interface depth obtained from Eq. (12).

The test of the successive correction model of the mean SSH field are carried out by the following two cases: only altimetric data are assimilated in experiment 3-1 for the reference. In experiment 3-2, observation data are the same as in experiment 2-2 where 32 drifting buoys (expt 1-4) and the altimetric data are assimilated simultaneously. In both cases, the 1-year-aver-

aged interface depth of the simulation run (Fig. 3b) is used for the initial guess of the mean field.

The time series of the rms errors for the interface depth are shown in Fig. 13. The error of the mean interface depth field corrected at each assimilation period is shown in Fig. 14. Experiment 3-2 using both the drifting buoy and the altimetric data shows a much smaller error than experiment 3-1. The instantaneous error decreases less than a half of the initial field, and the error in the mean interface depth field is also steadily reduced to 38.7 m, corresponding to a 40% reduction after the 1-year experiment (Fig. 15). This implies that the velocity data derived from the drifting buoys ensure the success of correcting the mean SSH and reducing the mean interface depth error leads to a better result of the assimilation experiment.

In contrast, the instantaneous error field in the case of assimilating only altimetric data (expt 3-1) cannot correct the mean interface depth field and the instantaneous field does not change from experiment 2-1. The error of the mean interface depth increases at the first assimilation time. This is due to the inconsistency in the mean field and the time-varying part of the altimetric observation, which increases the error in the analysis field [h^a in Eq. (23)]. The mean interface depth field at the scale of the gyre circulation cannot be corrected in this case, and this result is consistent with Marshall (1985) that assimilation of the altimetric data alone cannot separate the error in the model and in the mean field.

The generation of gravity waves shown in experiment 2 is reduced by the correction of the mean interface depth. The time evolution of the velocity error at 35°N, 142.5°E in experiment 3-2 is shown in Fig. 16. It appears that the gravity waves are reduced especially in the latter half of the experiment compared to those in experiment 2-2 (Fig. 12). This result shows that the inconsistency between the observed time-varying part and the estimated mean field is reduced through the

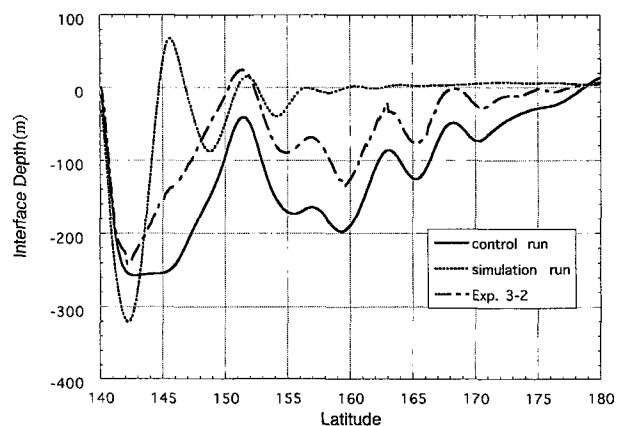


FIG. 17. Mean interface depth along 35°N in control run, simulation run, and expt 3-2.

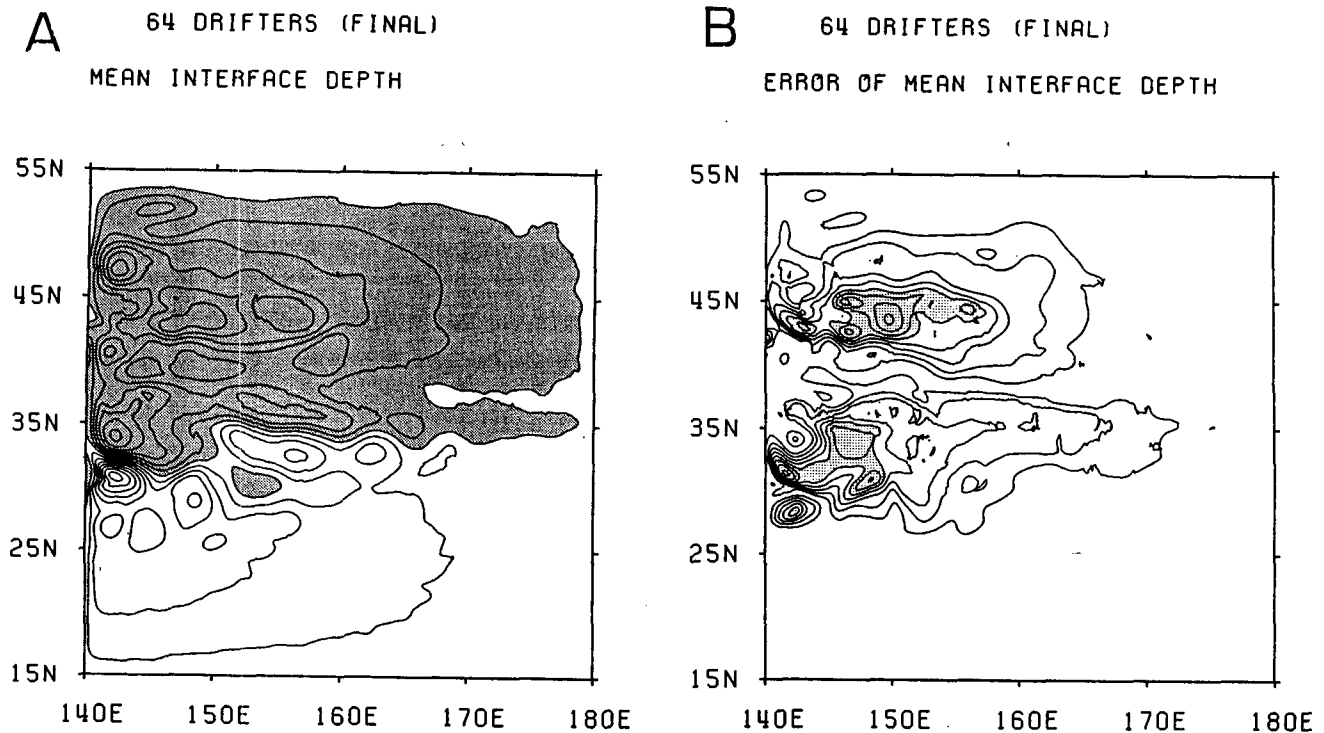


FIG. 18. As in Fig. 15 but for the experiment that assimilates 64 buoys and altimetric data into the model.

experiment. Some effects of gravity waves remain because the assumptions in the error covariance matrices (namely, a Gaussian distribution and the geostrophic balance) are insufficient and introduce the noise to the analysis field especially in the strong current-region.

4. Summary and discussion

The successive correction model of the mean SSH field is confirmed to work well with the simultaneous assimilation of drifting buoy and altimetric data. In particular, the velocities derived from the drifting buoys play an essential role in correcting the mean SSH field. As pointed out by Marshall (1985), the altimetric data assimilation alone cannot correct the mean SSH field. This problem is avoided in this study by the simultaneous assimilation of the drifting buoy data that is independent of the altimetric data. In addition, the correction of the mean SSH minimizes the inconsistency between the time-varying component derived from the altimetric data and the mean SSH field derived from the model average or climatological data. It also leads to the reduction of the gravity wave generation that tends to contaminate model results.

While the mean SSH field is corrected by the simultaneous assimilation of the drifting buoy data and the altimetric data, our present model is very simple and remains to be improved. The error of the mean interface depth corrected after the 1-year experiment is

reduced by approximately 40% of the initial guess field. The reasons for the remaining errors are likely due to the following factors. The estimated mean interface depth of experiment 3-2 along 35°N is very similar to that of control run (Fig. 17) except in the western boundary region. It means that the gradient of the mean interface depth, which is closely related to the surface circulation, is estimated well for scales of several hundred kilometers, although the absolute value is different from the true one. The error of the estimated mean interface depth gradient in experiment 3-2 is 0.26 m (km)^{-1} , while that in the simulation run is 0.47 m (km)^{-1} . Second, the number of the assimilated data is too small. Figure 18 shows the map of the estimated mean interface depth and its error for the experiment carried out for 1 year using 64 buoys, twice as many as used in experiment 3-2. In experiment 3-2, there are regions with a small error reduction in the subpolar gyre due to the small number of buoys in the region. In the case of 64 buoys, the error in the subpolar gyre is significantly reduced and the rms error of the mean interface depth field decreases to 35.4 m.

Another error source is associated with the assumption in the assimilation procedure, namely, a Gaussian correlation for the interface depth error and the geostrophic relationship between the interface depth error and the velocity error in the calculation of the error covariance matrix. This inadequate assumption produces a dynamical inconsistency in the analysis field

and generates gravity waves as is shown in Fig. 16. The gravity waves do not dissipate until the next assimilation period. These waves contaminate the model field and are likely to reduce the effectiveness of assimilation. To suppress such waves the assimilation scheme needs to be improved, such as using Kalman filter (e.g., Fukumori and Malanotte-Rizzoli 1995) that determines the error covariance matrix according to the model dynamics. Mariano (1990), on the other hand, introduced the method of combining geophysical fields using contour analysis to avoid smearing the dynamical features. Our assimilation scheme should be improved to be more sophisticated in order to gain better estimation of the mean SSH field as well as to suppress the gravity waves.

The impact of the assimilation model on the different number and initial deployment of the drifting buoys is also examined. It is confirmed that the drifting buoy data constrain both the velocity and the SSH fields in the model and can improve the accuracy of the estimated mean SSH field. The deployment of the drifting buoys affects the results of the assimilation. It is more effective when the drifting buoys exist in the western region because the assimilation of the velocity data in the strong current regions corresponds to the input of large energy and can affect the model output efficiently. These are quite useful not only for assimilation modeling but for planning the observation systems. In addition, the western region has large errors associated with the strong current and the fluctuations and buoys in this region correct the error more effectively than in small error regions.

The effectiveness of drifting buoy excursion is confirmed by comparison with a case using moored data. The excursion of the drifting buoys is effective in carrying the information in addition to the circulation advection and wave propagation. This suggests that broader spatial coverage is preferred to constrain the mean field rather than the dense coverage in time associated with the model predictability, consistent with Holland and Malanotte-Rizzoli (1989). It also can be explained by considering the degree of freedom of the observed data. The moored velocity data do not move geographically and the dynamical relationship of the time series data is strong. So the degree of freedom of the moored data is smaller than that of drifting buoy data, which is driven by the "true" velocity. The effectiveness of the drifting buoys in the western boundary current region is also explained by the long excursion due to the strong current.

The major cause for the increasing rms error during the last 100 days of assimilation (Figs. 6 and 9) is that a great number of drifting buoys have gone away from the energetic western boundary current region, where assimilation of the buoy-derived velocities into the model effectively corrects the model error. In addition to the small kinetic energy of the observed velocity data during the last 100 days of assimilation mentioned ear-

lier (Fig. 8), this is confirmed by the time series of the velocity errors in the western boundary regions. For example, the time series of the velocity errors at 35°N, 142.5°E in experiment 1-4 are shown in Fig. 19. The distance between each buoy and this point is also shown in the figure. The error decreases as the drifting buoys approach near this point before day 250. After day 250, with no arrival of the drifting buoys, the error accumulates steadily until around day 350. The time series of the normalized rms errors in experiments 1-1, 1-2, and 1-3, which have sparser buoy deployment in the western boundary current regions than experiment 1-4, show that the normalized rms errors increase up to 1.0 after day 300, indicating that the buoy data assimilation cannot constrain the model because of the small energy input by the nudging term after day 250. Although the normalized rms error in experiment 1-4 remains 0.7 at the end of the experiment (after one year), the error is also expected to finally approach 1.0 because of the escape of the drifting buoys from the western boundary current region. To confirm this, experiment 1-4 was extended for another one year. In addition, we performed another assimilation experiment in which the drifting buoy location after one year for experiment 1-4 is reset to their initial state and tracked for another one year, considering the fact that

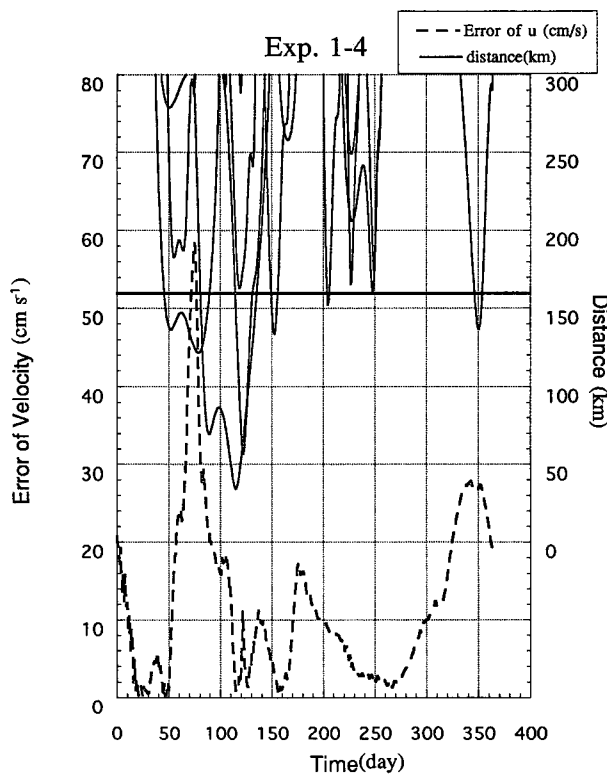


FIG. 19. Time series of the zonal velocity errors at a fixed point (35°N, 142.5°E) (left axis) and those of distances between each buoy and this fixed point (right axis) in expt 1-4.

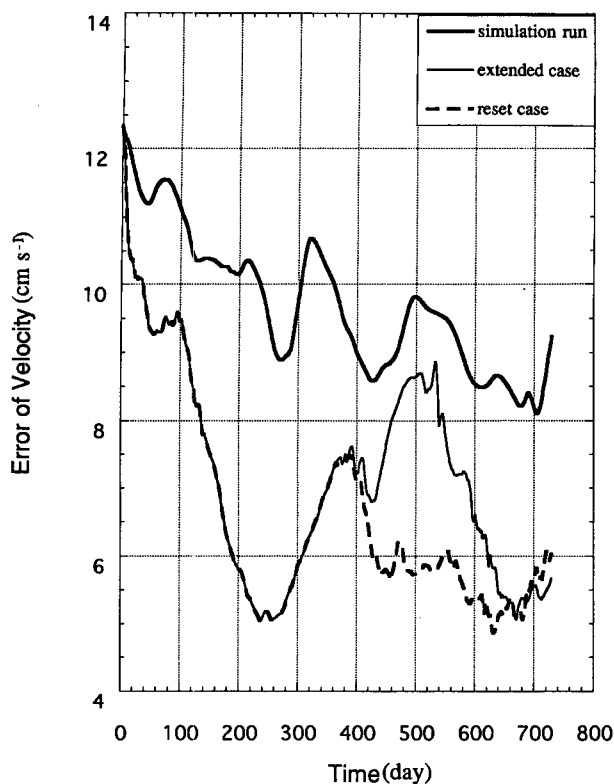


FIG. 20. Time series of the rms errors for zonal velocity in the case that expt 1-4 is extended for another one year (thin solid line), and in the case that the drifting buoy location is reset to the initial state after the 1-year calculation in expt 1-4 (dotted line). Thick solid line indicates those in simulation run.

the mean lifetime of actual drifting buoys is about one year. The time series of the rms errors for the zonal velocity are shown in Fig. 20. As expected, the rms error in experiment 1-4 increases to the similar error level to that of the simulation run around day 550. After then, the error decreases because some of the buoys recirculate back to the western boundary current region. In contrast, in the case that the drifting buoys are redistributed, the rms error rapidly decreases, reaching the error level on day 600 similar to that of experiment 1-4 on day 250.

In this study, the model-simulated data are assimilated as the observed data without considering the observation errors. Clearly, the observation errors cannot be ignored when real data are assimilated. The assimilation scheme used in this study can be used for real data including observation errors, although errors in the analysis field and estimated mean SSH field will likely increase. The observation errors in the buoy velocities are more important than those in the altimetric data because the velocity data constrain the gradient of the SSH and success of the model in this study is ensured by the assimilation of the velocity data. The observation errors in the drifting buoy data are primarily due

to satellite positioning error, which corresponds to about $2\text{--}3\text{ cm s}^{-1}$ for daily velocity observations. Components in the drifting buoy data that the numerical model does not include are also regarded as observation errors, such as thermohaline circulation, sub-grid scale phenomena, Ekman transport, and tides. These errors are difficult to evaluate quantitatively, but some parts of the errors can be reduced by improving the model.

The experiment in this study shows the success of the successive correction model of the mean SSH field with simultaneous assimilation of the drifting buoy and altimetric data. While there is no observation error and the result may be somewhat optimistic, the effectiveness of the assimilation of the independent data is shown. We speculate that assimilation models including the subsurface hydrographic field will be very useful and development of such models should be pursued. Inclusion of subsurface hydrographic data can also be used to estimate the mean SSH field. The model in this study will be improved to include the deep ocean and thermodynamical effects.

Acknowledgments. The authors express their thanks to Drs. Motoyoshi Ikeda, Norihisa Imasato, and Roger Lukas for helpful discussions. We also thank two anonymous reviewers for their invaluable comments and suggestions. The numerical calculation was carried out on FACOM VP2600/10E and M1800 at the Data Processing Center of Kyoto University.

REFERENCES

- Awaji, T., K. Akitomo, and N. Imasato, 1991: Numerical study of shelf water motion driven by the Kuroshio: Barotropic model. *J. Phys. Oceanogr.*, **21**, 11–27.
- Capotondi, A., W. R. Holland, and P. Malanotte-Rizzoli, 1995: Assimilation of altimetric data into a quasigeostrophic model of the Gulf Stream system. Part II: Assimilation results. *J. Phys. Oceanogr.*, **25**, 1153–1173.
- Daley, R., 1991: *Atmospheric Data Analysis*. Cambridge University Press, 457 pp.
- Ezer, T., and G. L. Mellor, 1994: Continuous assimilation of Geosat altimeter data into a three-dimensional primitive equation Gulf Stream model. *J. Phys. Oceanogr.*, **24**, 832–847.
- , —, D.-S. Ko, and Z. Sirkes, 1993: A comparison of Gulf Stream sea surface height fields derived from Geosat altimeter data and those derived from sea surface temperature data. *J. Atmos. Oceanic Technol.*, **10**, 76–87.
- Fukumori, I., and P. Malanotte-Rizzoli, 1995: An approximate Kalman filter for ocean data assimilation: An example with an idealized Gulf Stream model. *J. Geophys. Res.*, **100**, 6777–6793.
- Ghil, M., and P. Malanotte-Rizzoli, 1991: Data assimilation in meteorology and oceanography. *Advances in Geophysics*, Vol. 33, Academic Press, 141–266.
- Haines, K., P. Malanotte-Rizzoli, R. E. Young, and W. R. Holland, 1993: A comparison of two methods for the assimilation of altimeter data into a shallow-water model. *Dyn. Atmos. Oceans*, **17**, 89–133.
- Holland, W. R., and P. Malanotte-Rizzoli, 1989: Alongtrack assimilation of altimeter data into an ocean circulation model: Space versus time resolution studies. *J. Phys. Oceanogr.*, **19**, 1507–1534.

- Kelly, K. A., and S. T. Gille, 1990: Gulf Stream surface transport and statistics at 69°W from the Geosat altimeter. *J. Geophys. Res.*, **95**, 3149–3161.
- Le Traon, P. Y., J. Stum, J. Doradeu, P. Gasper, and P. Vincent, 1994: Global statistical analysis of TOPEX and POSEIDON data. *J. Geophys. Res.*, **99**, 24 619–24 631.
- Malanotte-Rizzoli, P., and R. E. Young, 1992: How useful are localized clusters of traditional oceanographic measurement for data assimilation? *Dyn. Atmos. Oceans.*, **17**, 23–61.
- Mariano, A. J., 1990: Contour analysis: A new approach for melding geophysical fields. *J. Atmos. Oceanic Technol.*, **7**, 285–296.
- Marshall, J. L., 1985: Determining the ocean circulation and improving the geoid from satellite altimetry. *J. Phys. Oceanogr.*, **15**, 330–349.
- Mellor, G. L., and T. Ezer, 1991: A Gulf Stream model and an altimetry assimilation scheme. *J. Geophys. Res.*, **96**, 8779–8795.
- Nerem, R. S., E. J. Sctama, C. J. Kobinsky, and B. D. Beckley, 1994: A preliminary evaluation of ocean topography from the TOPEX/POSEIDON mission. *J. Geophys. Res.*, **99**, 24 565–24 583.
- Qiu, B., 1994: Determining the mean Gulf Stream and its recirculations through combining hydrographic and altimetric data. *J. Geophys. Res.*, **99**, 951–962.
- , K. A. Kelly, and T. M. Joyce, 1991: Mean flow and variability in the Kuroshio extension from Geosat altimetry data. *J. Geophys. Res.*, **96**, 18 491–18 507.
- Rapp, R. H., Y. Yi, and Y. M. Wang, 1994: Mean sea surface and geoid gradient comparison with TOPEX altimeter data. *J. Geophys. Res.*, **99**, 24 657–24 667.
- Stammer, D., and C. Wunsch, 1994: Preliminary assessment of the accuracy and precision of TOPEX/POSEIDON altimeter data with respect to the large-scale ocean circulation. *J. Geophys. Res.*, **99**, 24 584–24 604.
- White, W. B., C.-K. Tai, and W. R. Holland, 1990: Continuous assimilation of simulated Geosat altimetric sea level into an eddy-resolving numerical ocean model. Part 1. Sea level differences. *J. Geophys. Res.*, **95**, 3219–3234.
- Willebrand, J., R. H. Käse, D. Stammer, H.-H. Hinrichsen, and W. Krauss, 1990: Verification of Geosat sea surface topography in the Gulf Stream extension with surface drifting buoys and hydrographic measurements. *J. Geophys. Res.*, **95**, 3007–3014.